Proceedings of the ASME 2018
Dynamic Systems and Control Conference
DSCC2018
September 30-October 3, 2018, Atlanta, Georgia, USA

DSCC2018-9004

DESIGN OPTIMIZATION OF RML GLOVE FOR IMPROVED GRASP PERFORMANCE

Teja Vanteddu
Robotics and Mechatronics Lab
Mechanical Engineering Dept.
Virginia Tech
Blacksburg, VA, USA
tejav@vt.edu

Bijo Sebastian
Robotics and Mechatronics Lab
Mechanical Engineering Dept.
Virginia Tech
Blacksburg, VA, USA
bijo7@vt.edu

Pinhas Ben-Tzvi
Robotics and Mechatronics Lab
Mechanical Engineering Dept.
Virginia Tech
Blacksburg, VA, USA
bentzvi@vt.edu

ABSTRACT

This paper describes the design optimization of the RML Glove in order to improve its grasp performance. The existing design is limited to grasping objects of large diameter (>110mm) due to its inability in attaining high bending angles. For an exoskeleton glove to be effective in its use as an assistive and rehabilitation device for Activities of Daily Living (ADL), it should be able to interact with objects over a wide range of sizes. Motivated by these limitations, the kinematics of the existing linkage mechanism was analyzed in detail and the design variables were identified. Two different cost functions were formulated and compared in their ability to yield optimal values for the design variables. The optimal set of design variables was chosen based on the grasp angles achieved and the resulting mechanism was simulated in CAD for feasibility testing. An exoskeleton mechanism corresponding to the index finger was manufactured with the chosen design variables and detailed experimental validation was performed to illustrate the improvement in grasp performance over the existing design. The paper ends with a summary of the experimental results and directions for future research.

1 INTRODUCTION

Over the past few decades, many exoskeleton gloves have been made by various companies and research labs [1]. Most of these exoskeleton gloves are intended for rehabilitation for victims suffering from partial or complete hand paralysis, with common causes including stroke or nerve damage due to traumatic injury. The exoskeleton gloves that have been designed for such applications can be broadly divided into two types: rigid and soft gloves. Rigid gloves have better force transmission and can achieve the desired grasp configurations more easily [2-10]. Cybergrasp is used for tele-manipulation or grasping computer generated objects [2]. The SAFER glove uses PCB as the rigid linkage and generates fingertip force trajectories using GMR method [3]. Underactuated serial linkage mechanism was used which can exert high forces [4-5]. OFX uses a pneumatic actuation system to drive the finger mechanism [6]. A combination of rigid linkage and Bowden cable mechanism was used to drive the glove using Series Elastic Actuators (SEA) [7]. Inspired by the human finger skeletal structure, a 3 degree of freedom linkage mechanism was designed actuated by SEA [8]. HANDEXOS was designed so that each finger can be actuated independently using linkage mechanism driven by cables [9]. Planar three link mechanism which attaches to user finger at a single point and actuated by a single motor is designed for HEXOSYS II [10]. However, they have their own disadvantages in that they are often heavy, bulky, and can hinder the natural motion of the hand. Soft

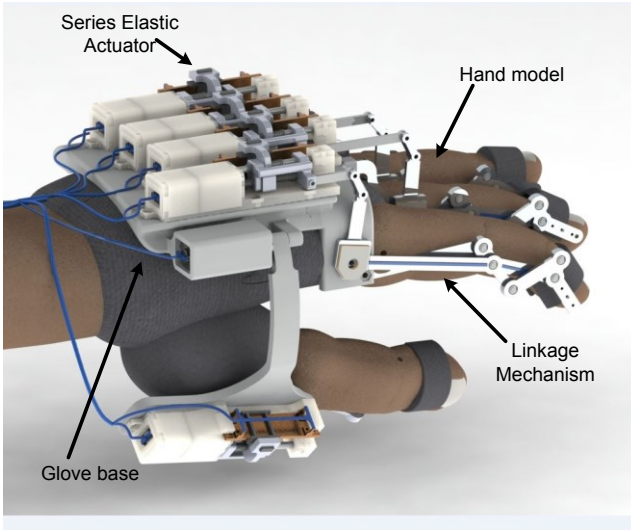

Figure 1. RML glove

gloves on the other hand are actuated using cables in different ways including routing through thermoplastic guides [11], anchoring about thimble like straps and using soft tendon routing mechanism [12] and use of Bowden cable system to keep the actuation system at a remote location [13]. Special inflatable polymers have also been used to build soft gloves which can bend to produce the grasping motion desired. There are several materials and types of actuation methods like actuation using pneumatics which will bend upon pressurization [14], air muscles integrated with a linkage [15], molded elastomeric chambers which bend upon applying fluid pressure [16-17] and can be adjusted to different finger lengths [18]. The soft gloves compared to their rigid counterparts are lightweight and less bulky. Nevertheless, there are major disadvantages as well including less effective transmission of force as the tendons face frictional losses, natural bending trajectories are difficult to obtain from soft polymers, and bulky actuation systems are often required, especially in the case of pneumatically actuated gloves.

In order to address the challenges faced by the state of the art gloves, Refour et al. designed an exoskeleton glove [19], hereafter referred to as the RML Glove. The distinguishing factor of this design was the use of a linkage mechanism slim enough to fit between the fingers, resulting in a lightweight, low profile system. In addition, each finger of the glove was designed to be a single degree of freedom (DoF) mechanism, allowing them to be actuated using a single motor while following a trajectory modelled after a healthy human hand. The design and the inner workings of the RML Glove are explained in detail in [19].

This paper focuses on the design optimization of the existing RML Glove mechanism in order to enable grasping of small diameter objects using the glove. Results of the experimental validation performed as part of the previous work have shown that the existing glove design cannot produce finger trajectories required for grasping cylindrical objects with a diameter less than 100 mm. For the glove to be effective in its use as an assistive and rehabilitation device, it must be able to grasp objects with a wide range of sizes. This is the major motivation behind the design optimization described in this paper.

The approach followed in this paper is as follows; the kinematics of the linkage mechanism is analyzed and the design variables are chosen. The cost function for optimization is formulated so as to maximize the mechanism's ability to grasp objects of varying sizes. Finally, the mechanism is optimized over the design space to find the values of the design variables that maximize the cost function.

This paper is divided into six sections. Section 2 describes the kinematics of the linkage, including analytical formulations for the trajectory produced by the mechanism. Section 3 defines the optimization problem and describes the approach in detail. Section 4 shows the comparison between the different cost functions and also shows the improvement in the operative range obtained after optimization over the existing design. In Section 5, the results obtained in Section 4 are experimentally validated. Section 6 concludes the paper and provides direction for future research.

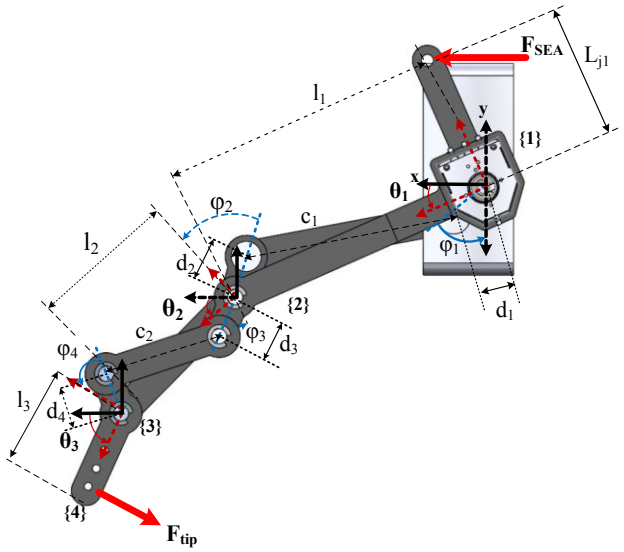

Figure 2. Kinematic model

2 KINEMATICS REVIEW

In order to optimize the design variables, it is necessary to obtain analytical relationships between the design variables and the corresponding joint angles produced by the mechanism. This is done through the kinematic modeling of the mechanism as shown in Fig. 2. The kinematic modelling of the mechanism was originally conducted in [19] using multi-body modelling techniques. This same model is used to derive the analytical expressions as described below.

As shown in Fig. 2, the various symbols used are l_1, l_2 and l_3 for link lengths, c_1 and c_2 for constraint link lengths, θ_1, θ_2 and θ_3 for joint angles and φ_1, φ_2, φ_3, φ_4 for the angles of constraint joints with respect to the global y-axis.

Below are the constraint equations relating link parameters and the angles at each joint:

$$\begin{aligned} c_1^2 = {} & [l_1\cos\theta_1 - d_2\sin\phi_2\cos\theta_2 - d_2\cos\phi_2\sin\theta_2 - d_1\sin\phi_1]^2 \\ & + [l_1\sin\theta_1 - d_2\sin\phi_2\sin\theta_2 + d_2\cos\phi_2\cos\theta_2 - d_1\cos\phi_1]^2 \end{aligned} \quad (1)$$

$$\begin{aligned} c_2^2 = {} & [(l_1 + d_3\sin\phi_3\cos\theta_1) - (-d_3\cos\phi_3\sin\theta_1) - l_1\cos\theta_1 \\ & - l_2\cos\theta_2 - (-d_4\sin\phi_4\cos\theta_3) + d_4\cos\phi_4\sin\theta_3]^2 \\ & + [(l_1 + d_3\sin\phi_3\sin\theta_1) - (-d_3\cos\phi_3\cos\theta_1) - l_1\sin\theta_1 \\ & - l_2\sin\theta_2 - (-d_4\sin\phi_4\sin\theta_3) + d_4\cos\phi_4\cos\theta_3]^2 \end{aligned} \quad (2)$$

These constraint equations are solved for a given θ_1 to find expressions for θ_2 and θ_3. The analytical expressions for θ_2 and θ_3 are given below:

$$\theta_2 = \sin^{-1}\left(\frac{B_1C_1 - \sqrt{A_1^4 + A_1^2B_1^2 - A_1^2C_1^2}}{A_1^2 + B_1^2}\right) \quad (3)$$

where,

$$A_1 = 2d_1d_2\sin\varphi_1\sin\varphi_2 - 2l_1d_2\sin\varphi_2\cos\theta_1 + 2d_1d_2\cos\varphi_1\cos\varphi_2 + 2l_1d_2\cos\varphi_2\sin\theta_1$$

$$B_1 = 2d_1d_2\sin\varphi_1\cos\varphi_2 - 2l_1d_2\cos\varphi_2\cos\theta_1 - 2d_1d_2\cos\varphi_1\sin\varphi_2 - 2l_1d_2\sin\varphi_2\sin\theta_1$$

$$C_1 = c_1^2 - (l_1^2 + d_1^2 + d_2^2 - 2l_1d_1\sin\varphi_1\cos\theta_1 + 2l_1d_1\cos\varphi_1\sin\theta_1)$$

$$\theta_3 = \sin^{-1}\left(\frac{B_2C_2 - \sqrt{{A_2}^4 + {A_2}^2{B_2}^2 - {A_2}^2{C_2}^2}}{{A_2}^2 + {B_2}^2}\right) \quad (4)$$

where,

$$A_2 = 2Bd_4\cos\varphi_4 - 2Ad_4\sin\varphi_4$$

$$B_2 = -2Ad_4\cos\varphi_4 - 2Bd_4\sin\varphi_4$$

$$C_2 = c_2^2 - (A^2 + B^2 + d_4^2)$$

$$A = l_1\cos\theta_1 + l_2\cos\theta_2 - ((l_1 + d_3\sin\varphi_3)\cos\theta_1 + d_3\cos\varphi_3\sin\theta_1)$$

$$B = l_1\sin\theta_1 + l_2\sin\theta_2 - ((l_1 + d_3\sin\varphi_3)\sin\theta_1 - d_3\cos\varphi_3\cos\theta_1)$$

Using the above formulation, for a given θ_1 and link parameters l_1, l_2, l_3, d_1, d_2, d_3, d_4, φ_1, φ_2, φ_3 and φ_4, we can calculate θ_2 and θ_3. The link lengths have been selected based on previous studies on human hand anatomy as described in [19]. The dimensions were chosen such that they provide a comfortable fit for an averaged size adult male. With these parameters fixed, the optimization will be performed on the following design variables, d_1, d_2, d_3, d_4, φ_1, φ_2, φ_3 and φ_4 for larger values of θ_2 and θ_3.

3 APPROACH

Any optimization process involves the following; an objective or cost function, design variables and the linear and non-linear constraints to be followed during the optimization. The optimization process itself will try to find the values for the design variables that maximize the objective function while satisfying the constraints.

As mentioned above, the design variables are the link parameters d_1, d_2, d_3, d_4, φ_1, φ_2, φ_3 and φ_4. The non-linear constraints are described in the previous section as part of the kinematic model Eq. (1-2). The optimization function used in the previous design was a weighted sum of squared error of joint angles θ_1, θ_2 and θ_3 between from kinematic model and biomechanical data on the trajectory of a human grasp.

Joint angles produced by a healthy human hand as obtained from previous medical studies were used to optimize the previous design. This allowed the design to produce natural motion on the users' hand when wearing the glove. The limitation of this cost function was that it did not optimize the linkage for large bending angles, as it tries to optimize for the complete grasp trajectory. This produces values for the design variables that satisfy all the points on the trajectory on average.

This inference clearly motivates the need to change the objective function formulation so as to achieve our goal of larger grasp angles. Based on this requirement, two objective functions have been formulated, as described in the following section. The design variables produced by both methods are compared in simulation to decide upon the best of the two choices.

The cost function chosen for this investigation is the weighted sum of errors for the end position of the grasp trajectory between the kinematic model and the HUST (Huazhong University of Science and Technology) dataset, defined as the position at which the lead screw is at its maximum extension. For this fixed θ_1, the link parameters are optimized so as to improve θ_2 and θ_3 bending angles. The difference between this cost function and the one described in the previous work is the fact that for the new cost function error variable is calculated only for the final position.

In addition, the joint angles for the desired grasp trajectories were obtained from a study of various grasp taxonomies [20]. According to this study, there are broadly 33 types of grasps based on the objects we handle in our daily life. Our requirement dictates a grasp with high bending angles. The grasps that approximate our requirement were the small diameter (Grasp number 2 in the study) and lateral grasps (Grasp number 16). The quantitative data for the two grasps were obtained from Handcorpus Company. The study performed by the company [21] involves all the 33 grasps, compiled in a dataset called the HUST dataset. The study involves 30 subjects, each having performed all the 33 grasps. After comparing between the small diameter grasp and lateral grasp, the latter was found to have higher bending angles. For the rest of the paper we use this data for the optimization process. In order to obtain optimal values of the design variables, two different cost functions are proposed.

The first cost function for the optimization problem is given by the minimization of *F(x)*, where:

$$F(x) = w_1e_1 + w_2e_2 \quad (5)$$

In the above expression, w_1 and w_2 are the weighting parameters, and e_1 and e_2 are the absolute errors of θ_2 and θ_3, respectively. Linear inequality constraints are applied on the design variables, with d_1, d_2 and d_4 having a lower limit of 7 mm and upper limit of 13 mm, while d_3 has a lower limit of 6 mm and upper limit of 10 mm. The upper bound for d_3 is selected to minimize protrusion into the grasp space, as it is on the side where the object will be grasped. As d_1, d_2 and d_4 do not protrude into the grasp space when grasping an object, the upper bounds for those segments are higher than for d_3. The lower limits are selected such that the constraining joint is not close enough to interfere with joint 2 and 3. In the case of the constant joint angles, φ_1, φ_2, φ_3 and φ_4 have upper limits of 80 degrees, while φ_2, and φ_4 have lower limits of 10 degrees. Additionally, φ_1 has a lower limit of 20 degrees and φ_3 has a

lower limit of 30 degrees. For the angle φ_3, the lower limit is selected in order to prevent the constraint joint from protruding beyond the width of the finger. This prevents the mechanism from causing any obstruction while grasping any object. The remaining angles φ_1, φ_2 and φ_4 have lower limits compared to φ_3, as they do not obstruct when grasping an object.

The second cost function tested is defined as the error in Euclidean distance of the tip of the linkage for the end position of the grasp trajectory between the kinematic model and the HUST data. The optimization problem is a minimization of $G(x)$, where $G(x)$ is given below:

$$G(x) = \sqrt{(x_k - x_h)^2 + (y_k - y_h)^2} \tag{6}$$

In the above expression, x_k and y_k are tip coordinates of link l_3 calculated from θ_1, θ_2 and θ_3 obtained from the kinematic model derived in the previous section. x_h and y_h are tip coordinates of link l_3 calculated from joint angles obtained from a specific grasp in the HUST dataset. The linear and non-linear constraints are the same as in the previous cost function case. Both of these cost functions are convex functions so this becomes a convex optimization problem.

4 ANALYSIS

Optimization is performed for both cost functions separately for a lateral grasp, as given by the HUST dataset using interior point algorithm available in the MATLAB function *fmincon*. Figures 3, 4 and 5 show the results for the non-optimized case, the mechanism optimized with first cost function and the mechanism optimized with second cost function, respectively. Based on the optimization results as shown in Figs. 3, 4 and 5, there is significant improvement in achieving larger grasp angles following optimization as compared to the existing mechanism. Table 1 provides quantitative data for comparing the two cost functions.

As shown in Table 1, the second cost function achieves larger grasp angles with lower percentage error for both θ_2 and θ_3. Based on the above results, the second cost function is chosen for the analysis. The values of optimized design variables are {d_1-12.9, d_2-7, d_3-9.4, d_4-7.5 mm}, {φ_1-20.6, φ_2-76.7, φ_3-40.7, φ_4-44.7 degrees}. A more intuitive representation of the results is apparent from the improvement in the size of objects that can be grasped with the new optimized linkage. An approximate cylinder size was fitted in CAD software

Table 1: Comparison of the two cost functions

	θ_2	θ_3
Target angles (Degrees)	108.2	158.3
Angles achieved with 1st cost function	83.4	130.8
Percent error	-22.9	-17.3
Angle achieved with 2nd cost function	105.7	160.3
Percent error	-2.3	1.3

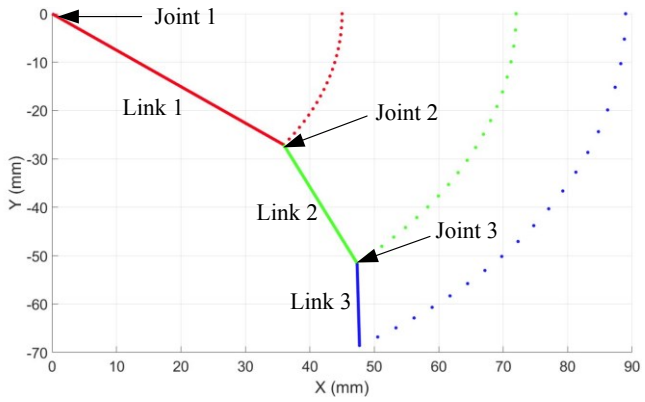

Figure 3. Final position of the linkage before optimization

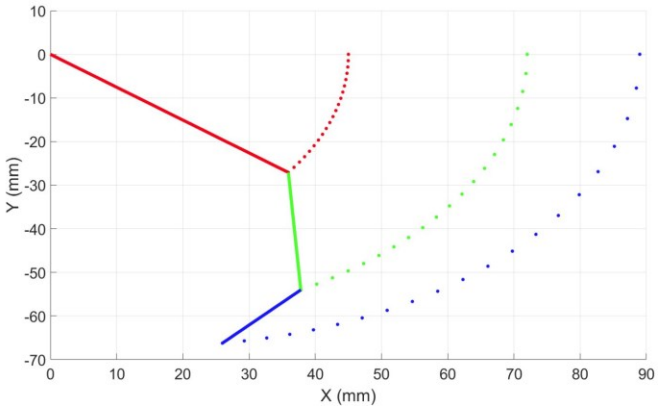

Figure 4. Final position of the linkage after optimization with 1st cost function

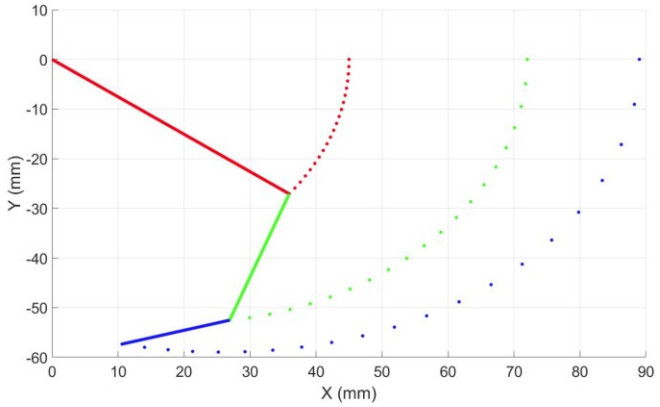

Figure 5. Final position of linkage after optimization with 2nd cost function

such that the cylinder is touching and tangent to all three links. The minimum possible diameter of the body is measured to check the quantitative improvement in grasp angles. Table 2 provides information on the percentage improvement in the object sizes that can be grasped for various values of θ_1.

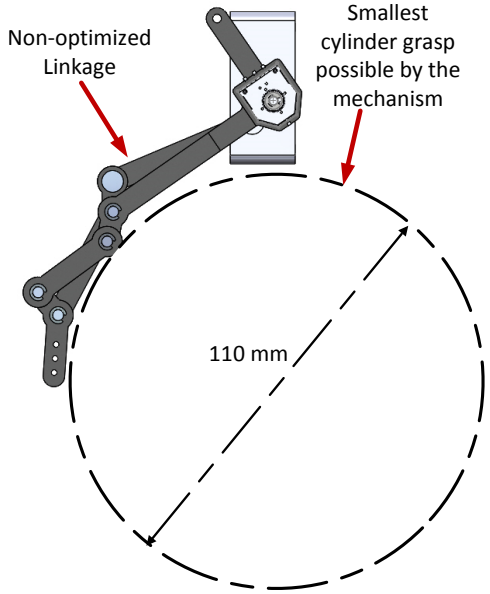

Figure 6. Smallest cylinder fit possible for the non-optimized linkage

Table 2: Improvement in object size that can be grasped

	Object size (Dia. in mm)		
θ_1(Degrees)	Non optimized	Optimized	% Improvement
27.9	136.3	50.7	62.8
29.8	131.2	48.7	62.9
31.7	127.0	47.1	62.9
33.5	123.0	45.6	62.9
35.4	120.0	44.4	63.0

Figures 6 and 7 show visual representation of the minimum possible cylinder grasp that can be achieved by the mechanism for both cases of optimized and non-optimized linkages, respectively. For the existing non-optimized case, the mechanism reaches its maximum bending limit with a cylinder grasp of diameter 110 mm. The optimized mechanism on the other hand can accommodate a cylinder grasp with a diameter as small as 36 mm. In addition, the improvement in grasping time is compared for the same θ_3 angle between the non-optimized and optimized case. The joint angle θ_3 drives the majority of the percentage of the grasp reached. This assumption is validated by checking the sensitivity in change of the object size by varying θ_2 alone and then θ_3 alone, the results of which are shown in Table 3. From the data in Table 3, the change in object size that can be grasped is higher for θ_3 compared to θ_2.

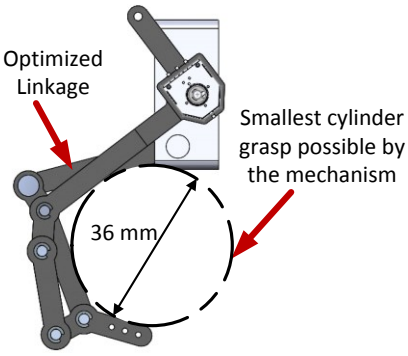

Figure 7. Smallest cylinder fit possible for the optimized linkage

Table 3: Sensitivity analysis of θ_2 and θ_3 on object size

	Original object size(mm)	Object size for 10 degrees change in θ_2	Object size for 10 degrees change in θ_3
Case 1	123.0	121.6	101.5
Case 2	136.3	134.9	110.7
Case 3	45.6	44.6	41.5
Case 4	50.7	50.0	45.7

Table 4: Improvement in grasping time of optimized linkage over non-optimized linkage

θ_3 (Degrees)	Existing mechanism(s)	Optimized mechanism(s)	% Improvement
-57.1	1.1	0.5	56.4
-61.2	1.2	0.5	56.7
-65.2	1.3	0.6	56.9
-83.0	1.8	0.7	61.1
-86.1	1.9	0.8	57.9
-89.1	2	0.8	60.0

While comparing the θ_1 values required for achieving the same θ_3 position in both the non-optimized and optimized case, the improvement in grasp time is proportional to the ratio of θ_1 values. Table 4 represents the improvement in time of closure for different values of θ_3. It is assumed that joint 1 is moving at a constant angular velocity of 0.32 rad/s. The calculations show there is roughly a 60% improvement in time taken to reach a particular grasp.

In order to establish the usefulness of the proposed mechanism as an assistive device, the tip force must be calculated for the optimized linkage to ensure it falls within the acceptable range. Tip force determines the maximum weight of the object that can be grasped without any slippage, to ensure safe handling. In order to determine the tip force, the analytical relation between the input force from motor and the output tip force is derived below.

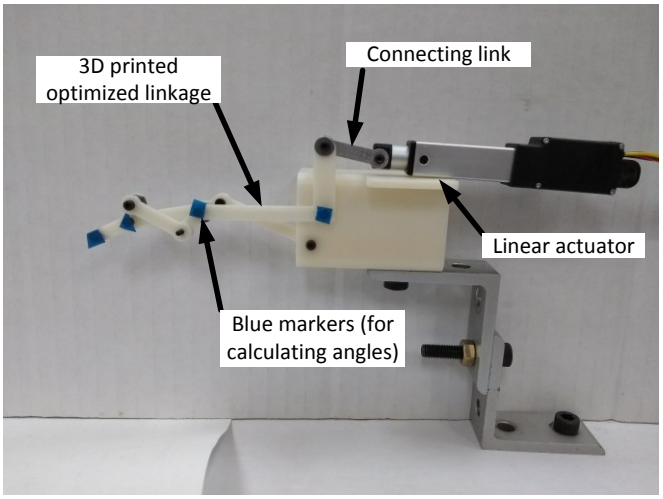

Figure 8. Experiment setup with linear actuator in retracted position

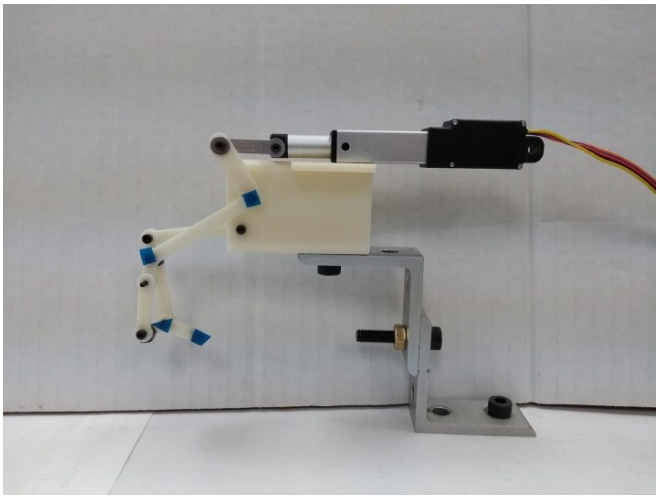

Figure 9. Experiment setup with linear actuator in extended position

The principle of virtual work was used to determine the tip force, as expressed below:

$$T\partial\theta_1 = F_{tip}\partial r \tag{7}$$

In the above expression, T is the torque applied at joint 1. F_{tip} is the force applied by the glove on the object being grasped and is assumed to be acting perpendicular to link 3 at its tip and r is the tip position of link 3. Eq. (7) is differentiated with respect to time and is solved for F_{tip} using the kinematic relations derived in Section 2.

$$F_{tip} = \frac{T\theta_1\sqrt{(y_4 - y_3)^2 + (x_3 - x_4)^2}}{x_f + y_f} \tag{8}$$

where,

$$x_f = (x_2\theta_1 + (x_3 - x_2)\theta_2 + (x_4 - x_3)\theta_3)(x_4 - x_3)$$
$$y_f = (-y_2\theta_1 + (y_2 - y_3)\theta_2 + (y_3 - y_4)\theta_3)(y_3 - y_4)$$

In the above expression (x_1, y_1), (x_2, y_2) and (x_3, y_3) are the position coordinates of joint 1, 2 and 3, respectively. x_4 and y_4 is the position coordinate of the tip of link 3 where the force, F_{tip} is applied.

$$\theta_2 = K\theta_1$$
$$K = \frac{B_{dyn}l_1\cos\theta_1 - A_{dyn}l_1\sin\theta_1}{(B_{dyn}d_2(\sin\varphi_2\cos\theta_2 + \cos\varphi_2\sin\theta_2) + A_{dyn}d_2(\cos\varphi_2\cos\theta_2 - \sin\varphi_2\sin\theta_2))}$$
$$A_{dyn} = 2(l_1\cos\theta_1 - d_2(\sin\varphi_2\cos\theta_2 + \cos\varphi_2\sin\theta_2) - d_1\sin\varphi_1) \tag{9}$$
$$B_{dyn} = 2(l_1\sin\theta_1 + d_2(\cos\varphi_2\cos\theta_2 - \sin\varphi_2\sin\theta_2) + d_1\sin\varphi_1)$$

It is assumed that there is no friction at the joints and the links are rigid. The tip force is calculated for the static case, where the linkages are not moving and are in a state of equilibrium.

$$\theta_3 = \frac{-(E + FK)\theta_1}{G}$$
$$E = C(d_3\sin\varphi_3\sin\theta_1 - d_3\cos\varphi_3\cos\theta_1) - D(d_3\sin\varphi_3\cos\theta_1 + d_3\cos\varphi_3\sin\theta_1)$$
$$F = l_2(-C\sin\theta_2 + D\cos\theta_2)$$
$$G = d_4(C(\sin\varphi_4\sin\theta_3 - \cos\varphi_4\cos\theta_3) - D(\cos\varphi_4\sin\theta_3 + \sin\varphi_4\cos\theta_3) \tag{10}$$
$$C = 2(l_1\cos\theta_1 + l_2\cos\theta_2 - d_4(\sin\varphi_4\cos\theta_3 + \cos\varphi_4\sin\theta_3) - ((l_1 + d_3\sin\varphi_3)\cos\theta_1 + d_3\cos\varphi_3\sin\theta_1))$$
$$D = 2(l_1\sin\theta_1 + l_2\sin\theta_2 + d_4(\cos\varphi_4\cos\theta_3 - \sin\varphi_4\sin\theta_3) - ((l_1 + d_3\sin\varphi_3)\sin\theta_1 - d_3\cos\varphi_3\cos\theta_1))$$

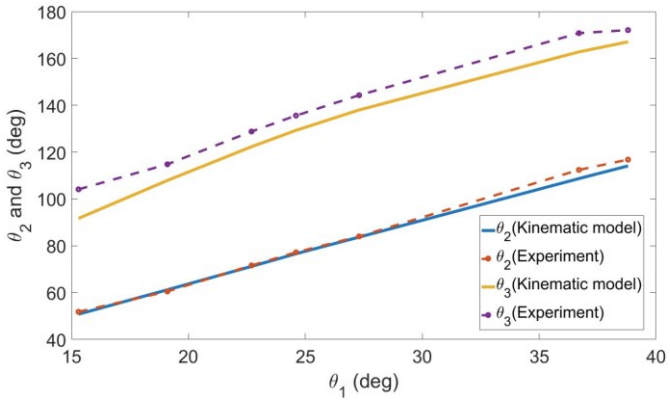

Figure 10. Comparison of θ_2 and θ_3 between kinematic model and experimental values

The tip forces calculated correspond to the case where the glove has grasped the object and is no longer moving. The force for maximum extended case, F_{tip} is calculated to be 32 N for θ_1 = 37 degrees. The tip force decreases as θ_1 decreases.

5 EXPERIMENTS

To validate the results of Section 4, a CAD model with the optimized design parameter values were made in SolidWorks. The joint angle values are compared between the SolidWorks model and the analytical solution. The percentage error for θ_2 was found to be less than 0.05 %, and for θ_3 less than 0.04 %. This demonstrates the kinematic model holds for all θ_1 values when compared with the CAD model, as the percent error is very small.

In order to experimentally validate the optimization results, the mechanism was 3D printed with the optimized design values. The mechanism was then assembled and fixed on a stand, and a linear actuator was attached. Blue markers placed on joints 1, 2 and 3 as well as on the tip of link 3 were used to track the joint trajectories produced by the mechanism. A calibrated camera was used to capture the linkage position at specified time intervals. Image processing algorithms were used to process the image and detect the blue markers. The detected markers were then connected with straight lines to approximate the linkages, and the corresponding joint angles were calculated from the results. The algorithm for joint angle calculation used here is same as detailed in [1].

Fig. 10 shows comparison of the θ_2 and θ_3 values between the kinematics model and the experiment. The percentage error is calculated to be below 10% for both θ_2 and θ_3. The presence of this error can be attributed to mechanical backlash in the joints, the effect of which becomes magnified over the length of the mechanism.

6 CONCLUSION AND FUTURE WORK

This paper detailed the design optimization of the RML Glove [1] in order to improve its grasp performance. Larger bending angles allow the glove to grasp objects of smaller dimension with ease; a major requirement for effective operation of assistive exoskeleton gloves. In order to improve upon the grasp angles produced by the glove mechanism, a design optimization was performed. Two cost functions were proposed and the results were compared to decide upon the best choice of design variables. In order to conduct the optimization, an analytical solution for the joint angles and joint velocities was derived in terms of the design variables. The analytical expression for calculating the tip force corresponding to a known input torque has also been derived. The results show that the optimized design can allow grasping of objects 63% smaller in size while also providing a grasp timing improvement by 60%.

Future work includes replicating this optimization process for all the fingers of the glove. There is further room for design optimization in the link connecting the leadscrew and the mechanism. Furthermore, the device can be optimized to achieve higher force transmission at likely grasp configurations, thus improving the tip force during grasping. Role of elasticity will be studied to perform energy consumption optimization for improving efficiency. Also grasp tests will be performed to determine the maximum size of the object that can be safely held using the glove.

REFERENCES

[1] R. Bogue and R. Bogue, “Exoskeletons and robotic prosthetics : a review of recent developments,” Ind. Robot An Int. J., vol. 36, no. 5, pp. 421–427, 2009.

[2] CyberGlove Systems LLC, “CyberGrasp,” 2009. [Online].Available:http://www.cyberglovesystems.com/cybergrasp/.

[3] P. Ben-Tzvi, J. Danoff, and Z. Ma, “The Design Evolution of a Sensing and Force-Feedback Exoskeleton Robotic Glove for Hand Rehabilitation Application,” J. Mech. Robot., vol. 8, no. 5, p. 51019, 2016.

[4] J. Iqbal, H. Khan, N. G. Tsagarakis, and D. G. Caldwell, “A novel exoskeleton robotic system for hand rehabilitation - Conceptualization to prototyping,” Biocybern. Biomed. Eng., vol. 34, no. 2, pp. 79–89, 2014.

[5] I. H. Ertas, E. Hocaoglu, D. E. Barkana, and V. Patoglu, “Finger exoskeleton for treatment of tendon injuries,” Proc. 11th IEEE Int. Conf. Rehabil. Robot. ICORR, pp. 194–201, 2009.

[6] P. Heo and J. Kim, “Power-assistive finger exoskeleton with a palmar opening at the fingerpad,” IEEE Trans. Biomed. Eng., vol. 61, no. 11, pp. 2688–2697, 2014.

[7] P. Agarwal, J. Fox, Y. Yun, M. K. O’Malley, and A. D. Deshpande, “An index finger exoskeleton with series elastic actuation for rehabilitation: Design, control and performance characterization,” Int. J. Rob. Res., vol. 34, no. 14, pp. 1747–1772, Dec. 2015.

[8] I. Jo and J. Bae, “Design and control of a wearable and force-controllable hand exoskeleton system,” Mechatronics, vol. 41, no. c, pp. 90–101, Feb. 2017.

[9] A. Chiri et al., “HANDEXOS: Towards an exoskeleton device for the rehabilitation of the hand,” in 2009 IEEE/RSJ International Conference on Intelligent Robots and Systems, 2009, pp. 1106–1111.

[10] J. Iqbal, O. Ahmad, and A. Malik, “HEXOSYS II - towards realization of light mass robotics for the hand,” in 2011 IEEE 14th International Multitopic Conference, 2011, pp. 115–119.

[11] SangWook Lee, K. A. Landers, and Hyung-Soon Park, “Development of a Biomimetic Hand Exotendon Device (BiomHED) for Restoration of Functional Hand Movement Post-Stroke,” IEEE Trans. Neural Syst. Rehabil. Eng., vol. 22, no. 4, pp. 886–898, Jul. 2014.

[12] H. In and K. Cho, “Exo-Glove : Soft wearable robot for the hand using soft tendon routing system,” IEEE Robot. Autom., vol. 22, no. March 2015, pp. 97–105, 2015.

[13] C. J. Nycz, M. A. Delph, and G. S. Fischer, “Modeling and design of a tendon actuated soft robotic exoskeleton for hemiparetic upper limb rehabilitation,” Proc. Annu. Int. Conf. IEEE Eng. Med. Biol. Soc. EMBS, vol. 2015–Novem, pp. 3889–3892, 2015.
[14] H. K. Yap, Jeong Hoon Lim, F. Nasrallah, J. C. H. Goh, and R. C. H. Yeow, “A soft exoskeleton for hand assistive and rehabilitation application using pneumatic actuators with variable stiffness,” in 2015 IEEE International Conference on Robotics and Automation (ICRA), 2015, pp. 4967–4972.
[15] I. Koo, B. Byunghyun Kang, and K.-J. Cho, “Development of Hand Exoskeleton using Pneumatic Artificial Muscle Combined with Linkage,” J. Korean Soc. Precis. Eng., vol. 30, pp. 1217–1224, 2013.
[16] P. Polygerinos, Z. Wang, K. C. Galloway, R. J. Wood, and C. J. Walsh, “Soft robotic glove for combined assistance and at-home rehabilitation,” Rob. Auton. Syst., vol. 73, pp. 135–143, 2015.
[17] P. Polygerinos et al., “Towards a soft pneumatic glove for hand rehabilitation,” in 2013 IEEE/RSJ International Conference on Intelligent Robots and Systems, 2013, pp. 1512–1517.
[18] S.-S. Yun, B. B. Kang, and K.-J. Cho, “Exo-Glove PM: An Easily Customizable Modularized Pneumatic Assistive Glove,” IEEE Robot. Autom. Lett., vol. 2, no. 3, pp. 1725–1732, Jul. 2017.
[19] Refour, E., Sebastian, B., Ben-Tzvi, P., “Two-Digit Robotic Exoskeleton Glove Mechanism: Design and Integration”, Journal of Mechanisms and Robotics, Transactions of the ASME, Vol. 10, Issue 2, pp. 025002: 1-9, April 2018.
[20] T. Feix, J. Romero, H. B. Schmiedmayer, A. M. Dollar and D. Kragic, "The GRASP Taxonomy of Human Grasp Types," in IEEE Transactions on Human-Machine Systems, vol. 46, no. 1, pp. 66-77, Feb. 2016.
[21] “HUST Dataset (March 2016).” *HandCorpus*, www.handcorpus.org/?p=1596.